SPANWISE WALL OSCILLATION CONTROL OF COMPRESSIBLE CHANNEL FLOW

Marius Ruby
Chair of Fluid Dynamics
University of Siegen
57072 Siegen
marius.ruby@uni-siegen.de

Holger Foysi
Chair of Fluid Dynamics
University of Siegen
57072 Siegen
holger.foysi@uni-siegen.de

ABSTRACT

This contribution deals with an active control method for wall-bounded flows with the aim to lower the turbulence intensity and thus the wall friction drag. The resulting flow is altered in the near wall region and demands less energy to be driven against the viscous forces. Numerical simulations are used for the investigations with a specific velocity distribution imposed at the wall. The latter is directed in the spanwise direction and varies in the streamwise direction in a sinusoidal fashion. This velocity modulation is derived from the classic time dependent wall oscillations and closely related to it, when regarding the resulting flow (Viotti *et al.* (2009)). The control method is applied to compressible channel flow where different combinations of Mach and Reynolds numbers $Ma_b = [0.3\ 1.5\ 3.0]$ and $Re^*_{\tau c} = [150\ 400\ 800]$ are studied yielding friction Reynolds numbers up to Re_τ =2500. Higher drag reduction is achieved in the supersonic cases linked to variable density compressibility effects. The control method is furthermore applied to a more real-world configuration, in that it is applied to a jet flow emanating out of round pipe. The pipe wall is subject to the wall movement similar to the ones used in the channel flow configurations, with a jet exit Reynolds number of $Re = v_{xc}d/\mu_w = 16000$ (based on diameter d and peak velocity v_{xc}) and the Mach number $Ma_b = 0.3$. Effects of the control on jet properties like streamwise evolution and shear layer development are studied and compared to the unaffected flow.

INTRODUCTION

While oscillatory control techniques have been overwhelmingly studied in imcompressible flow, the aforementioned method is applied to compressible supersonic channel flow in this work, building upon work by Ruby & Foysi (2022). Strong gradients of viscosity, density and temperature arise under these conditions, affecting also the efficiency of the control method. The method of operation is basically the same in compressible conditions and it is observed that drag reduction levels of similar order can be achieved compared to incompressible flow. To reveal the differences in more detail, though, and to ascribe them to compressibility with sufficient confidence, it is necessary to have comparable data of quite a few different Mach-/Reynolds numbers and control parameters. Key findings of the available dataset include a larger net power saving at the higher Mach numbers and an increased value of the optimum control wavelength (Ruby & Foysi, 2022). Furthermore the premultiplied one- and two-dimensional spectra are studied to see the effect of the control as well as compressibility on the size of the structures, stresses or Reynolds stress budget quantities.

The second case of application comprises a jet flow emanating out of a round pipe. The pipe section, subject to the present oscillation control, was first investigated experimentally by Auteri *et al.* (2010). The effect on different turbulence levels at the nozzle exit on the jet development was scrutinized numerically in Barré *et al.* (2006) and Brès *et al.* (2018) for example. Few works include the nozzle geometry or use only a short length resulting in insufficient flow development at the nozzle exit. Here, a large section of 16 times the pipe diameter is used to study the effect of a lowered turbulence level due to the oscillation control on the jet flow.

CONTROL METHOD

The control method used in this work can be categorized into oscillatory flow control. An overview of this type of flow control can be found in Ricco *et al.* (2021), for example. The general aim is to lower the turbulent part of the friction drag. This is done by imposing any form of oscillations in order to weaken the momentum transfer between the high velocity and near wall region. Spanwise oscillatory wall motion (Touber & Leschziner (2012)), streamwise (longitudinal) travelling waves of spanwise velocity (Quadrio *et al.* (2009)) or even spanwise travelling transversal waves through flexible surfaces (Roggenkamp *et al.* (2015)) are possible means for that.

The oscillation technique used in the proposed project is based on an approach by Viotti *et al.* (2009), who transformed the time dependent spanwise wall motion with velocity W,

$$W = A\sin(2\pi t/T), \tag{1}$$

into a pure space dependent formulation

$$W = A\sin(2\pi x/\Lambda_x), \tag{2}$$

with time t, oscillation amplitude A and period T. In Eq. (2), x denotes the streamwise coordinate and the time period T from Eq. (1) is converted into a wavelength Λ_x in that streamwise direction. A sketch of this configuration is given in Figure 1.

This conversion is possible because the flow exhibits a quasi-universal convection velocity in the thin near-wall layer, where the wall velocity makes an impact, therefore, the flow already exhibits a temporal structure. Together with a spatial variation along the convection direction, an observer travelling with the fluid experiences the same periodic spanwise movement described by Eq. (1). The control according to Eq. 2 can equally be interpreted as a standing wave based on the terminology in Quadrio *et al.* (2009). Although the new configuration is not easily transferable to experimental settings (the wall would have to be replaced by separate treadmills of opposing directions) it is conceivable of being implemented by an appropriate surface manipulation due to its static nature. Thanks to the missing necessity to perpetually alter the spanwise direction of the flow in time, both the power to drive the flow (associated with drag reduction) and the expended power was shown to be substantially lowered compared to the temporal case (Viotti *et al.* (2009)). This gives rise to a positive net energy budget for a broad range of parameters.

COMPRESSIBLE CHANNEL FLOW

Nature of compressible flow

Owing to several transformations available it is possible to compare a compressible flow to the correspondent incompressible one if the flow parameters are chosen appropriately. However, due to substantial variations of viscosity, density, and temperature within the near-wall region in supersonic flow, it is difficult to find corespondent incompressible conditions that matches it in all facets.

A useful quantity that is used in this regard is the semi-local Reynolds number that uses local values of viscosity and density and accounts for the majority of differences due to compressibility (Foysi *et al.* (2004); Patel *et al.* (2016)). An overview and comparison of different compressibility transformation rules for wall distance, mean velocity and Reynolds stresses is given in Modesti & Pirozzoli (2016). A good collapse of all these quantities could be found using the various transformations with the exception of the peak of the streamwise turbulent stress. It is higher than in the incompressible case as seen in many other studies (see e.g. Modesti & Pirozzoli (2016)).

Despite of the transformation rules, there are still some differences in the near-wall layer compared to incompressible flow, that can be purely attributed to compressibility or non-local effects. As the control method acts in this very layer, it is likely that the differences in efficiency are connected to the alterations by compressibility near the wall. Therefore, we not only compare the controlled flow in the various conditions, but also the uncontrolled reference flows to find reasons for different control efficiencies. Another possibility is to prescribe specific volume forces for the energy equation, too, accounting for variable property effects and, therefore, attenuating the differences as described above. This strategy is pursued for example in Gattere *et al.* (2023). Here, however, we intend the results to be able to be compared to experimental results or apply it to more realistic examples like a jet flow emanating from a round pipe. A body force wouldn't allow us to properly compare the results to possible future experiments.

Flow Conditions

To better compare compressible flow configurations to incompressible ones, a semi-local scaling (indicated by a $*$) is used here (Huang *et al.*, 1995; Foysi *et al.*, 2004). It tries to account for the aforementioned variation of thermodynamic quantities throughout the channel and associated effects. The semi-local Reynolds number

$$Re_\tau^* = Re_\tau \sqrt{\frac{\langle\rho\rangle}{\langle\rho_w\rangle}} \frac{\langle\mu\rangle}{\langle\mu_w\rangle} \tag{3}$$

was reformulated to show its connection to the incompressible counterpart Re_τ via an additional factor $\sqrt{\langle\rho\rangle\ \langle\rho_w\rangle}\langle\mu\rangle/\langle\mu_w\rangle$, with $\langle\cdot\rangle$ denoting a quantity averaged in time and over homogeneous directions, viscosity μ, density ρ and associated wall values μ_w and ρ_w. $Re_{\tau c}^*$ in turn indicates its value at the channel center. The bulk Mach number is defined by

$$Ma_b = U_b/c_w\,, \tag{4}$$

where c_w is the speed of sound at the wall and U_b is the bulk velocity, averaged in time and over all three directions.

The present data set obtained by the compressible flow solver PyFR (Witherden *et al.*, 2014) contains all combinations of $Ma_b = [0.3\ 1.5\ 3.0]$ and $Re_{\tau c}^* = [150\ 400\ 800]$ yielding friction Reynolds numbers up to 2500. An overview of the uncontrolled simulations is given in table 1. They serve as initial conditions for the controlled cases. Slight variations of the box sizes were necessary to fit integer multiples of various control wavelength in. Results of a smaller subset can be found in Ruby & Foysi (2022). The variation of the semi-local Reynolds number and local Mach number is demonstrated in figures 3 and 4 for the three different bulk Mach numbers and $Re_{\tau c}^* = 800$, exemplarily. A strong variation in the semi-local Reynolds number due to the steep gradient of viscosity and density addressed in the previous section is seen for the supersonic cases. At the channel center the supersonic Reynolds numbers coincide with the nearly incompressible case with $Ma_b = 0.3$, which shows hardly any variation over the wall-normal coordinate. On the other hand, a clear variation in local Mach number can be observed due to strong variations in temperature.

Affected and non affected cases share the same bulk Mach and bulk Reynolds numbers. The actuation amplitude according to Eq. 2 is $A^+ = 12$ for all controlled cases and streamwise wavelength Λ_x^* as single control parameter is scaled by the length scale $\delta_\nu^* = \langle\nu\rangle/u_\tau^*$ with $u_\tau^* = \sqrt{\tau_w/\langle\rho\rangle}$ using values for the local density and viscosity at the channel center.

Control Influence

In our previous paper (Ruby & Foysi, 2022) inital comparisons of the efficiency and successful application to supersonic channel flow was demonstrated. As an example for its suitability, selected normal components of the Reynolds stresses are depicted in Figure 5, exemplarily for $Ma_b = 3.0$ and $Re_{\tau c}^* = 800$, for all investigated control parameters. To give an impression how the near-wall flow is affected by the control method, the vortical structures are visualized with aid of the Q-criterion in Fig. 2. The sinusoidal pattern corresponding to two wavelengths is present in the streamwise dimension of the domain and visible in the near-wall flow. The spanwise velocity generation can be observed until about $y^* = 20$, where

$$y^* = \langle\rho\rangle\, y(\tau_w/\langle\rho\rangle)^{1/2}/\langle\mu\rangle \tag{5}$$

is the semi-local wall distance according to Huang *et al.* (1995). The spanwise wall velocity decays to almost zero throughout all flow conditions and control parameters at this wall distance. The length scales are altered in the controlled flow within the region of influence of the control. Shorter coherent low-speed / high-speed streaks become apparent due to disruption by the spanwise wall motion. This shift can be observed in frequency space by means of the premultiplied two-dimensional spectra (figure 7, left). Furthermore, the impact is not only confined to the direct near-wall region, as the one-dimensional spectra dependent on the wall-normal coordinate (figure 7, right) suggest. While the semi-local scaling is good at matching the key characteristics of compressible flows and their incompressible counterparts, there is still a discrepancy between compressible / incompressible length scales in the viscous sublayer (Patel *et al.*, 2016) that persists in the actuated flows likewise. This is demonstrated with aid of instantaneous velocity fluctuations in that region in figure 6. u'' denotes the Favre fluctuation regarding the mean $\widetilde{u} = \langle \rho u \rangle / \langle \rho \rangle$ and $u_\tau^* = \sqrt{\tau_w / \langle \rho \rangle}$ is the friction velocity derived by making use of the local density. Less locally intense fluctuations are visible in the higher Mach number flow, which additionally helps in providing a higher drag reduction of $1 - C_f/C_{f0} = 41\%$ in case $Ma_b = 1.5$, compared to 35% only in the nearly incompressible case. $C_f = 2\tau_w/(\rho_b U_b^2)$ denotes the skin friction coefficient and C_{f0} is the value of the unaffected flow. Furthermore, we find a correlation between the performance improvements at higher Mach numbers and the level of the pressure-strain term reduction (figure 8).

JET FLOW

In a second application, we investigate the jet flow emanating out of a round pipe with aid of implicit large eddy simulations using the flow solver PyFR (Witherden *et al.*, 2014). The same wall velocity distribution as in Eq. 2 is applied to the pipe where W corresponds to the circumferential direction now. The configuration is shown in figure 9 (a).

The jet exit Reynolds number based on pipe diameter d and peak velocity v_{xc} amounts to $Re = v_{xc}d/\mu_w = 16000$ and the Mach number based on the bulk velocity of the pipe is set to $Ma_b = 0.3$. The pipe length amounts to $16d$ to ensure fully developed turbulence at the end of the pipe. The jet dimensions amount to $5d$ and $25d$ in the radial and streamwise directions, respectively. Characteristic non-reflecting Riemann invariant conditions together with a sponge forcing are used at the outflow boundaries. Turbulence is generated at the inlet of the pipe with aid of an extended Synthetic Eddy Method (Giangaspero *et al.*, 2021) using the turbulent length scales and Reynolds stress components of a reference periodic pipe flow simulation. A 3D representation of the uncontrolled jet is shown in figure 9 (b), where rapid transition to turbulence within the pipe is perceivable. In case of the controlled pipe, the streamwise varying circumferential wall velocity with an amplitude of 12 times the friction velocity $u_\tau = \sqrt{\tau_w/\rho_w}$ and an optimum streamwise wavelength $\Lambda_x = \pi/2\,d$ is applied to the pipe wall. A drag reduction rate $1 - C_f/C_{f0}$ of 40 % is achieved that way, where C_f and C_{f0} denote the skin friction coefficients of the actuated and non actuated flows, respectively. The oscillation control was applied to generate two distinct cases. For one case it was constructed to lead to zero circumferential wall velocity at the pipe exit ($v_{\varphi e} = 0$). In an additional controlled case the steady wall velocity distribution was phase shifted such that the maximum circumferential wall velocity coincides with the pipe exit ($v_{\varphi e} = 12u_\tau$).

Control effects

Resulting RMS values of the streamwise velocity averaged over the circumferential direction are shown in figure 9 (c) for the pipe section of the controlled case with $v_{\varphi e} = 0$. It demonstrates the evolution dependent on the streamwise direction with high values in the initial region of the synthetic turbulence generation and additionally the impact of the wall actuation on that quantity. Profiles of the RMS velocity at fixed streamwise position $x/d = -0.04$ near the pipe exit are depicted in figure 10. The magnitude of all components is significantly reduced over the radial direction in the controlled cases except for the circumferential component in close vicinity of the wall. The effect of the control on the initial shear layer and developing region of the jet is revealed in figure 11. Centerline and lipline profiles of both the mean and RMS streamwise velocity are presented for all investigated cases. A behaviour similar to Barré *et al.* (2006), who compared two jets with low and high turbulence levels at the nozzle exit, can be observed for the uncontrolled case and the controlled one with zero circumferential exit velocity. The mean velocity at the centerline decays more rapidly for the controlled case and the mean velocity at the lipline rises more slowly reaching slightly higher values. A higher peak in the centerline streamwise RMS velocity appears for the controlled case compared to the unaffected configuration. Additionally, at the lipline, the controlled cases show a less distinct peak that is further away from the pipe exit. The rms levels exceed the uncontrolled levels afterwards up to about $x/d = 10$. The second controlled case with circumferential velocity at the exit $v_{\varphi e} = 12u_\tau$ shows a later onset of the velocity decay at the centerline converging to the uncontrolled graph at $x/d \approx 10$. The peak of the lipline RMS level is reduced in this case compared to the unaffected jet. Spectra of pressure fluctuations on the lipline are compared in figure 11 (c) at a streamwise position of $x/d = 0.5d$ close to the pipe exit. A distinct peak is visibile for the controlled case with $v_{\varphi e} = 0$ at $St = fd/v_{xc} \approx 1.5$, similar to observations in Brès *et al.* (2018), for example. Both the uncontrolled and the controlled case with nonzero circumferential exit velocity show a similar trend with a less distinct peak which is located at lower frequencies. Here, however, the control amplifies the pressure fluctuations clearly over most of the spectrum.

CONCLUSION

A steady wall oscillation method was applied to compressible channel flow. Different Reynolds numbers are compared at the same bulk Mach number and the Mach number effect is studied based on configurations that share the same semi-local Reynolds number at the channel center. Based on the chosen strategy for comparison, an increased efficiency was found for the supersonic cases compared to the nearly incompressible cases at bulk Mach number $Ma_b = 0.3$. A drag reduction level of 41 % was achieved at $Ma_b = 1.5$ compared to 35 % in case of $Ma_b = 0.3$ at center Reynolds number $Re_{\tau c}^* = 800$ for example. The compressible controlled flow benefits from variable density compressibility effects that alter the Reynolds stress anisotropies through the pressure-strain term manifesting in increased streak coherence.

The control method was applied to pipe flow with free jet exit condition, too, where a drag reduction rate of 40 % is achieved within the pipe. The oscillation pattern at the pipe wall is placed in a way that the circumferential wall velocity is zero at the exit in one case and maximum with the value of the oscillation amplitude $A^+ = 12$ in another case. Results concerning the evolution of mean and RMS levels in the jet region suggest that the jet is predominantly influenced through the turbulence level and the pipe exit condition. The additional circumferential exit velocity is able to reduce the peak of the streamwise velocity RMS level close to the exit. Overall the behaviour of the jet in this case is closer to the unaffected flow. The wall oscillation pattern in the pipe region itself does not show noticeable effects on the developing jet region.

REFERENCES

Auteri, F., Baron, A., Belan, M., Campanardi, G. & Quadrio, M. 2010 Experimental assessment of drag reduction by traveling waves in a turbulent pipe flow. *Physics of Fluids* **22** (11).

Barré, S., Bogey, C. & Bailly, C. 2006 Computation of the noise radiated by jets with laminar/turbulent nozzle-exit conditions **1**.

Brès, G., Jordan, P., Jaunet, V., Le Rallic, M., Cavalieri, A., Towne, A., Lele, S., Colonius, T. & Schmidt, O. 2018 Importance of the nozzle-exit boundary-layer state in subsonic turbulent jets. *Journal of Fluid Mechanics* **851**, 83–124.

Foysi, H., Sarkar, S. & Friedrich, R. 2004 Compressibility effects and turbulence scalings in supersonic channel flow. *J. Fluid Mech.* **509**, 207–216.

Gattere, F., Zanolini, M., Gatti, D., Bernardini, M. & Quadrio, M. 2023 Turbulent drag reduction with streamwise travelling waves in the compressible regime.

Giangaspero, G., Witherden, F. D. & Vincent, P. E. 2021 Synthetic turbulence generation for high-order scale-resolving simulations on unstructured grids. *AIAA Journal* .

Huang, P., Coleman, G. & Bradshaw, P. 1995 Compressible turbulent channel flows: DNS results and modelling. *Journal of Fluid Mechanics* **305**.

Modesti, D. & Pirozzoli, S. 2016 Reynolds and Mach number effects in compressible turbulent channel flow. *International Journal of Heat and Fluid Flow* **59**, 33–49.

Patel, A., Boersma, B. J. & Pecnik, R. 2016 The influence of near-wall density and viscosity gradients on turbulence in channel flows. *Journal of Fluid Mechanics* **809**, 793–820.

Quadrio, M., Ricco, P. & Viotti, C. 2009 Streamwise-travelling waves of spanwise wall velocity for turbulent drag reduction. *Journal of Fluid Mechanics* **627**, 161–178.

Ricco, P., Skote, M. & Leschziner, M. 2021 A review of turbulent skin-friction drag reduction by near-wall transverse forcing. *Progress in Aerospace Sciences* **123**, 100713.

Roggenkamp, D., Jessen, W., Li, W. & Schröder, W. 2015 Experimental investigation of turbulent boundary layers over transversal moving surfaces. *CEAS Aeronautical Journal* **6**, 471–484.

Ruby, M. & Foysi, H. 2022 Active control of compressible channel flow up to $Ma_b = 3$ using direct numerical simulations with spanwise velocity modulation at the walls. *GAMM-Mitteilungen* **45** (1).

Touber, E. & Leschziner, M. A. 2012 Near-wall streak modification by spanwise oscillatory wall motion and drag-reduction mechanisms. *Journal of Fluid Mechanics* **693**, 150–200.

Viotti, C., Quadrio, M. & Luchini, P. 2009 Streamwise oscillation of spanwise velocity at the wall of a channel for turbulent drag reduction. *Physics of Fluids* **21** (11), 115109.

Witherden, F.D., Farrington, A.M. & Vincent, P.E. 2014 PyFR: An open source framework for solving advection–diffusion type problems on streaming architectures using the flux reconstruction approach. *Computer Physics Communications* **185** (11), 3028 – 3040.

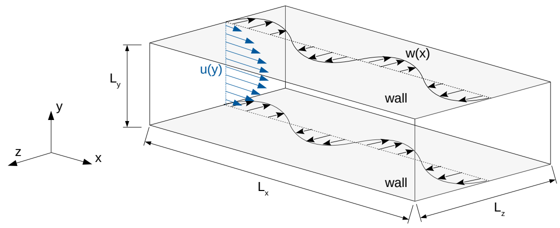

Figure 1. Sketch of the controlled channel flow configuration along with corresponding dimensions, directions and velocity distributions.

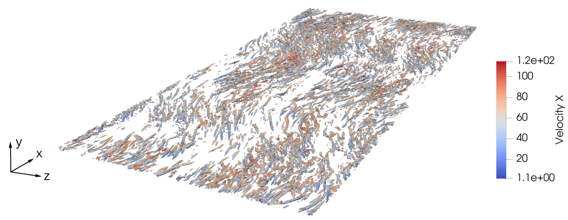

Figure 2. Near-wall vortices of a controlled flow ($Ma_b = 1.5$, $Re^*_{\tau c} = 400$), visualized by aid of the Q-criterion and coloured by the streamwise velocity.

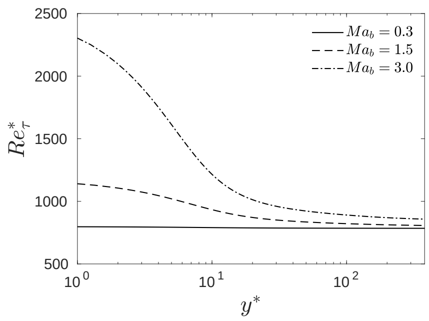

Figure 3. Wall-normal profiles of the semi-local Reynolds number Re^*_τ for three different bulk Mach numbers and equal center Reynolds number $Re^*_{\tau c} = 800$.

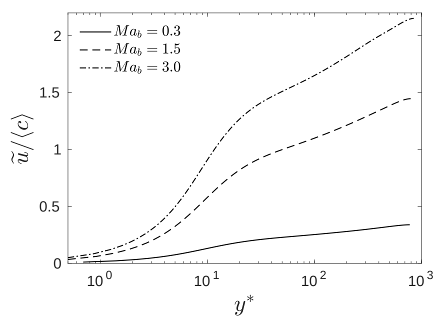

Figure 4. Wall-normal profiles of the local Mach number $\langle u \rangle / \langle c \rangle$ for three different bulk Mach numbers and equal center Reynolds number $Re^*_{\tau c} = 800$.

Ma_b	Re_b	Re_τ	$Re^*_{\tau c}$	$\frac{L_x \times L_z}{h}$	$N_x \times N_y \times N_z$	Δy^+	Δx^+	Δz^+
0.3	3000	192	188	$6\pi \times 2\pi$	$288 \times 128 \times 152$	$0.64 - 5.7$	12.6	7.9
1.5	3000	218	146	$6\pi \times 2\pi$	$288 \times 128 \times 152$	$0.73 - 6.5$	14.3	9.0
3.0	4880	454	148	$6\pi \times 3/2\pi$	$752 \times 224 \times 288$	$0.28 - 10.3$	11.3	7.4
0.3	6890	396	388	$3\pi \times \pi$	$300 \times 160 \times 200$	$0.63 - 11.1$	12.6	6.3
1.5	9450	604	407	$3\pi \times \pi$	$380 \times 200 \times 252$	$0.42 - 15.3$	15.1	7.5
3.0	14000	1150	398	$3\pi \times \pi$	$564 \times 336 \times 375$	$0.45 - 17.6$	19.3	9.6
0.3	15400	800	784	$2\pi \times \pi$	$400 \times 448 \times 400$	$0.71 - 6.8$	12.6	6.3
1.5	20000	1180	805	$2\pi \times \pi$	$396 \times 336 \times 396$	$0.46 - 18.0$	18.8	9.4
3.0	33035	2537	854	$2\pi \times \pi$	$800 \times 700 \times 800$	$0.58 - 22.4$	19.2	9.6

Table 1. Details of flow conditions, computational domains and grid resolutions of uncontrolled channel flow simulations.

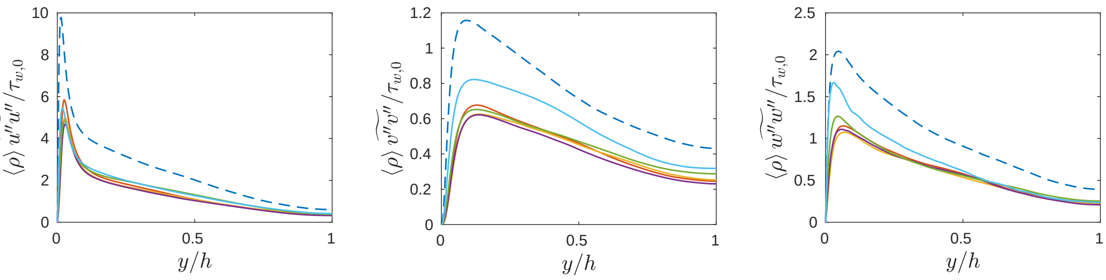

Figure 5. Impact of the control on turbulent momentum transfer, demonstrated for $Ma_b = 3.0$, $Re^*_{\tau c} = 800$. Dashed lines: uncontrolled flow, solid lines: different control parameters.

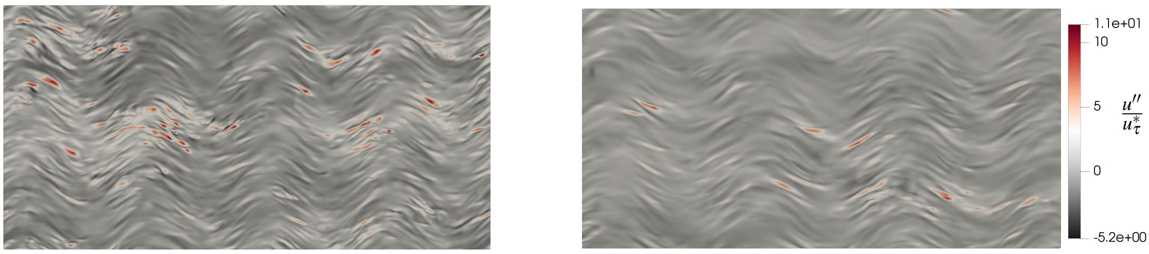

Figure 6. Instantaneous controlled velocity fluctuations in the wall-parallel plane at $y^* = 5$ for the nearly incompressible flow with $Ma_b = 0.3$ (left) and the supersonic flow with $Ma_b = 1.5$ (right). Reynolds number $Re^*_{\tau c}$ and control wavelength Λ^*_x amount to 800 and 1250, respectively, in both cases and the same size in semi-local units is shown.

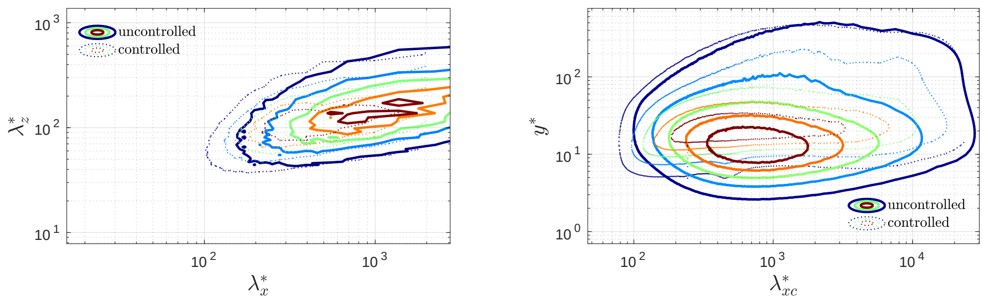

Figure 7. Left: Linearly spaced isocontours of the premultiplied two-dimensional spectra $k_x k_z E_{uu}(\lambda_x, \lambda_z)$ as functions of the wavelength vector $(\lambda_x, \lambda_z) = (2\pi/k_x, 2\pi/k_z)$ at $y^* = 20$ ($Ma_b = 1.5$, $Re^*_{\tau c} = 400$). Right: Linearly spaced isocontours of the one-dimensional spectra $k_x E_{uu}(\lambda_x)$ dependent on the wall-normal coordinate ($Ma_b = 0.3$, $Re^*_{\tau c} = 800$). Both the uncontrolled reference flow and a controlled flow with parameter $\Lambda^*_x \approx 1250$ is shown each time.

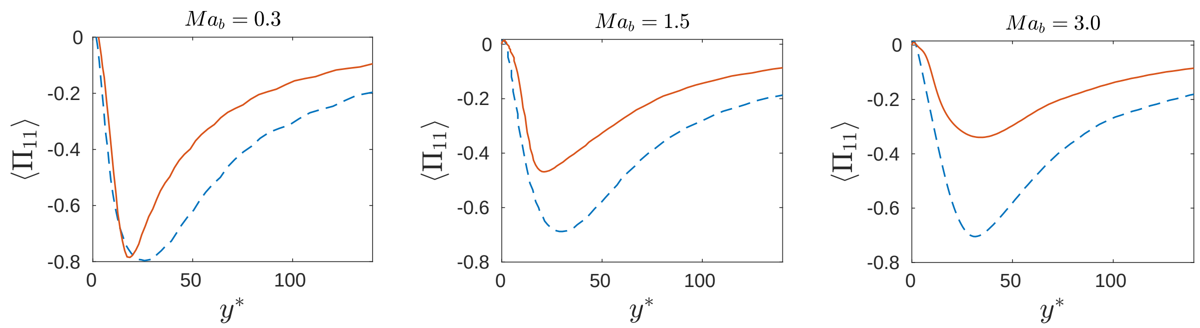

Figure 8. Pressure strain correlation $\Pi_{11} = \langle p' \partial u_1' / \partial x_1 \rangle - \langle \tau_{1j}' \partial u_1' / \partial x_j \rangle$ at three different Mach numbers Ma_b and $Re_{\tau c}^* = 400$ each for the uncontrolled (– – –) and a controlled flow (——) with parameter $\Lambda_x^* \approx 1250$.

Figure 9. (a) Sketch of the rotational symmetric pipe / jet flow configuration. (b) 3D representation of vorticity magnitude. (c) Evolution of the RMS streamwise velocity of the controlled case with $v_{\varphi e} = 0$ within the pipe.

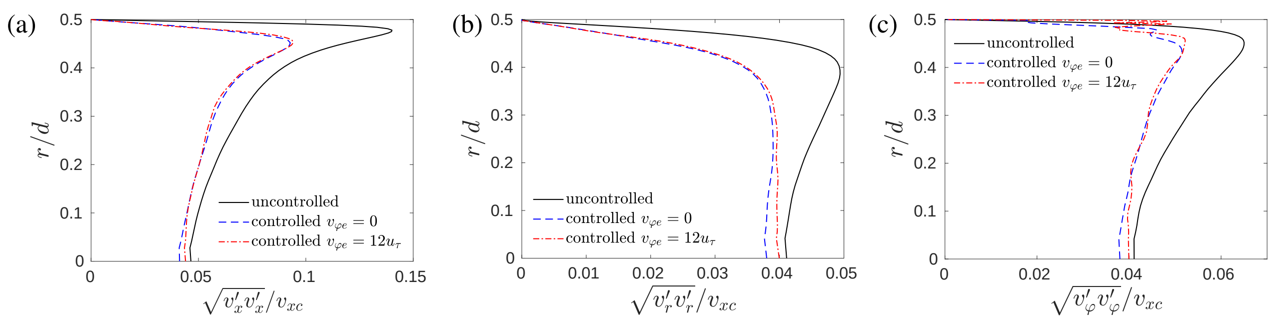

Figure 10. Profiles of streamwise (a), radial (b) and cimrcumferential (c) RMS velocities near the pipe exit at $x/d = -0.04$.

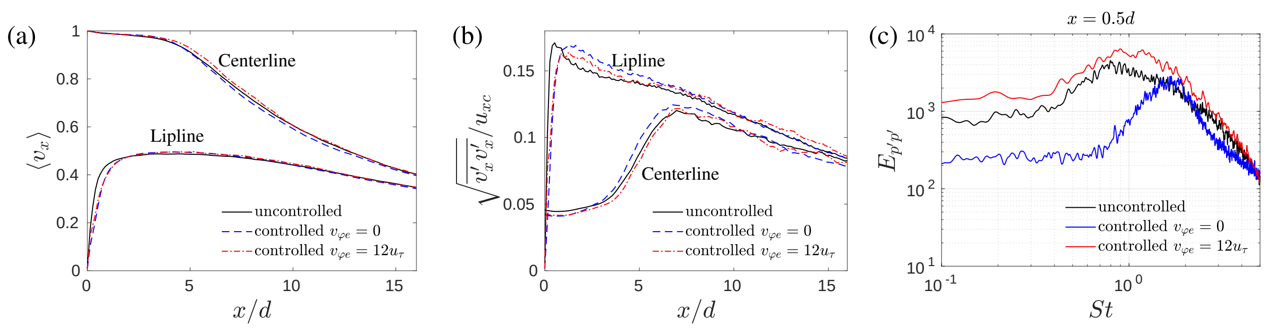

Figure 11. Centerline and Lipline of mean (a) and RMS (b) streamwise velocity in the jet region. (c) Spectra of pressure fluctuations on the lipline at streamwise position $x/d = 0.5$